Low-Complexity DOA Estimation of Noncircular Signals for Coprime Sensor Arrays

ZHAI Hui, CHEN Weiyang, ZHANG Xiaofei, ZHENG Wang*

College of Electronic and Information Engineering, Nanjing University of Aeronautics and Astronautics, Nanjing 210016, P. R. China

(Received 16 June 2018; revised 12 June 2019; accepted 4 July 2019)

Abstract: This paper presents a low-complexity method for the direction-of-arrival (DOA) estimation of noncircular signals for coprime sensor arrays. The noncircular property is exploited to improve the performance of DOA estimation. To reduce the computational complexity, the rotational invariance propagator method (RIPM) is included in the algorithm. First, the extended array output is reconstructed by combining the array output and its conjugated counterpart. Then, the RIPM is utilized to obtain two sets of DOA estimates for two subarrays. Finally, the true DOAs are estimated by combining the consistent results of the two subarrays. This illustrates the potential gain that both noncircularity and coprime arrays provide when considered together. The proposed algorithm has a lower computational complexity and a better DOA estimation performance than the standard estimation of signal parameters by the rotational invariance technique and Capon algorithm. Numerical simulation results illustrate the effectiveness and superiority of the proposed algorithm.

Key words: sensor array; direction of arrival estimation; coprime sensor arrays; noncircular signals; rotational invariance propagator method

CLC number: TN925 **Document code**: A **Article ID**: 1005-1120(2019)04-0599-10

0 Introduction

Over the last several decades, the direction-of arrival (DOA) estimation problem has received considerable attentions in the field of sensor array signal processing[1]. Many DOA estimation algorithms have been developed, including multiple signal classification (MUSIC)[2], estimation of signal parameters by the rotational invariance techniques (ESPRITs)[3], propagator method (PM)[4], and Capon algorithm[5]. PM does not require the eigenvalue decomposition (EVD) of covariance matrix, thus it has a smaller computational complexity[6]. But in conventional PM, the spectral peak search is used, while it still suffers from computational burden. To meet the real-time requirements, rotational invariance PM (RIPM) was proposed, which can avoid the spectral peak search.

In communication systems, noncircular (NC) signals have been widely used, such as amplitude modulation, binary phase shift keying, and quadrature phase shift keying modulated signals[7]. The NC feature has been widely used to enhance the performance of DOA estimation[8]. NC-MUSIC algorithm was proposed in Ref.[9], which showed that NC-MUSIC exceeds MUSIC in DOA estimation precision. Some modified algorithms were proposed to further improve DOA estimation performance based on NC feature[10-11]. However, these investigations are applied to the conventional arrays with inter-element spacing of half-wavelength.

Several studies have suggested that non-uniform linear arrays may outperform a uniform linear array (ULA) in terms of the number of sensors and resolution[12-13]. The inter-element spacing of non-

*Corresponding author, E-mail address: zhangxiaofei@nuaa.edu.cn.

How to cite this article: ZHAI Hui, CHEN Weiyang, ZHANG Xiaofei, et al. Low-Complexity DOA Estimation of Noncircular Signals for Coprime Sensor Arrays[J]. Transactions of Nanjing University of Aeronautics and Astronautics, 2019, 36(4): 599-608.

http://dx.doi.org/10.16356/j.1005-1120.2019.04.006

uniform linear arrays is larger than the half-wavelength. Thus, these non-uniform linear arrays have a larger aperture and better resolution than ULAs. Ref.[14] proposed a new non-uniform linear array called coprime sensor arrays (CSAs). A CSA can provide $O(N^2)$ degrees of freedom (DOFs) using just $O(N)$ sensors. This technique makes it possible to sample the spatial signals in a sparse way[15]. In Ref.[16], a method to estimate the DOAs was proposed by combing the results of the two subarrays of the CSA. In Ref.[13], a partial spectral peak search method was proposed for two-dimensional DOA estimation with coprime planar arrays. Li et al. proposed a real-valued cross correlation matrix method for coprime arrays[14]. However, the above-mentioned methods are all devised for circular signals, and no contributions have dealt yet with the problem of DOA estimation for CSAs assuming the signals to be NC.

In this paper, a computational efficiency method is proposed for the DOC estimation of NC signals for CSAs. The NC property is exploited to improve the performance of DOA estimation. To reduce the computational complexity, the NC rotational invariance propagator method (NC-RIPM) is included in the algorithm, which requires no spectral search and greatly reduces the complexity.

Our main contributions are as follows: (1) We consider noncircular signals impinging on a CSA and investigate the problem of DOA estimation in this new scenario. (2) We develop a NC-RIPM algorithm to reduce the computational complexity, which requires no spectral peak search. (3) The proposed algorithm has a better angle estimation performance than conventional methods for CSA. (4) The proposed algorithm requires no NC phase estimation, thus being more efficient in real-world application.

Notations: Lowercase (capital) bold symbols denote vectors (matrices). $(\cdot)^*$ and $(\cdot)^{\mathrm{T}}$ denote the complex conjugate and transpose, respectively, while $(\cdot)^{\mathrm{H}}$, $(\cdot)^{-1}$, and $\perp$ denote conjugate transpose, inverse, and ortho-complement of a projector matrix, respectively. diag$\{\boldsymbol{v}\}$ is a diagonal matrix whose diagonal is a vector $\boldsymbol{v}$. $E\{\cdot\}$ represents the statistical expectation. det$\{\cdot\}$, In$\{\cdot\}$, and Tr$\{\cdot\}$ are the determinant, the logarithm, and the trace operator of matrix, respectively. min$(\cdot)$ is to get the minimum element of an array. $\boldsymbol{I}_M$ represents an $M \times M$ identity matrix and $\boldsymbol{0}_{M\times N}$ is a zero matrix with $M \times N$. angle$(\cdot)$ means to get the phase.

1 Data Model

A CSA is constructed using two uniform linear subarrays with M and N sensors, respectively, where M and N are coprime integers, and the total number of elements is $M+N-1$. The subarray with M sensors (Subarray 1) has the inter-element spacing $N\lambda/2$, while the other subarray with N sensors (Subarray 2) has the inter-element spacing $M\lambda/2$. Fig.1 gives an example of a CSA.

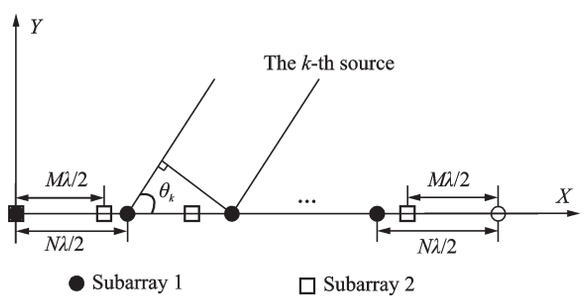

Fig.1 Illustration of the array geometry of a CSA

Assume that there are K far-field, uncorrelated narrow-band signals impinging on a CSA with $M+N-1$ antennas from angles $\boldsymbol{\theta}=[\theta_1,\theta_2,\cdots,\theta_K]$, where θ_k is the DOA of the k-th source, $k=1,\cdots,K$, and $K<\min\{M,N\}$. The noise is additive Gaussian with zero mean and variance σ^2, independent of the signals. For the unknown non-uniform noise scenario, the Ref.[17] formulated a reduced covariance tensor by exploiting the diagonal characteristic matrix to estimate the 2D DOA for uniform rectangle array. As the CSA can be decomposed into two uniform linear subarrays, the steering vectors corresponding to the k-th source for Subarrays 1 and 2 can be expressed as follows[15]

$$\boldsymbol{a}_1(\theta_k)=[1,\mathrm{e}^{\mathrm{j}\mu_{k,1}},\cdots,\mathrm{e}^{\mathrm{j}(M-1)\mu_{k,1}}]^{\mathrm{T}}\in\mathbf{C}^{M\times 1} \quad (1)$$

$$\boldsymbol{a}_2(\theta_k)=[1,\mathrm{e}^{\mathrm{j}\mu_{k,2}},\cdots,\mathrm{e}^{\mathrm{j}(N-1)\mu_{k,2}}]^{\mathrm{T}}\in\mathbf{C}^{N\times 1} \quad (2)$$

where $\mu_{k,1}=-\pi d_1\sin\theta_k/\lambda$, $d_1=N\lambda/2$, $\mu_{k,2}=-\pi d_2\sin\theta_k/\lambda, d_2=M\lambda/2$, and $k=1,\cdots,K$.

Then, the received signal vectors of Subarrays 1, 2 at the t-th time slot can be defined as[15]

$$\boldsymbol{x}_1(t)=\boldsymbol{A}_1\boldsymbol{s}(t)+\boldsymbol{n}_1(t) \tag{3}$$

$$\boldsymbol{x}_2(t)=\boldsymbol{A}_2\boldsymbol{s}(t)+\boldsymbol{n}_2(t) \tag{4}$$

where $\boldsymbol{A}_1=[\boldsymbol{a}_1(\theta_1),\cdots,\boldsymbol{a}_1(\theta_K)]\in\mathbf{C}^{(M-1)\times K}$ and $\boldsymbol{A}_2=[\boldsymbol{a}_2(\theta_1),\cdots,\boldsymbol{a}_2(\theta_K)]\in\mathbf{C}^{(N-1)\times K}$ are the steering matrices of Subarrays 1, 2, respectively. $\boldsymbol{s}(t)\in\mathbf{C}^{K\times 1}$ is the narrow-band NC signal vector, $\boldsymbol{n}_1(t)$ and $\boldsymbol{n}_2(t)$ denote the additive white Gaussian noise, and $t=1,\cdots,L$, L denotes the number of snapshots.

We just consider the maximum NC rate signal in this paper, the vector of NC signals can be expressed as follows[18]

$$\boldsymbol{s}(t)=\boldsymbol{\Psi}\boldsymbol{s}_0(t)\qquad t=1,\cdots,L \tag{5}$$

where $\boldsymbol{s}_0(t)\in\mathbf{R}^{K\times 1}$ and $\boldsymbol{\Psi}$ is a diagonal matrix, which is represented as follows

$$\boldsymbol{\Psi}=\begin{bmatrix}\mathrm{e}^{-\mathrm{j}\varphi_1} & & \\ & \ddots & \\ & & \mathrm{e}^{-\mathrm{j}\varphi_K}\end{bmatrix} \tag{6}$$

where φ_k is the NC phase of the k-th signal. According to Eqs.(3) and (5), the received vectors of Subarray 1 and Subarray 2 can be expressed as follows

$$\boldsymbol{x}_1(t)=\boldsymbol{A}_1\boldsymbol{\Psi}\boldsymbol{s}_0(t)+\boldsymbol{n}_1(t) \tag{7}$$

$$\boldsymbol{x}_2(t)=\boldsymbol{A}_2\boldsymbol{\Psi}\boldsymbol{s}_0(t)+\boldsymbol{n}_2(t) \tag{8}$$

2 DOA Estimation Algorithm

In this section, we derive the NC-RIPM algorithm for the DOA estimation of NC signals for CSA. We first give the extended data model by exploiting the NC property, then discuss about the NC-RIPM algorithm and phase ambiguity problem. And finally, in the last part of this section, the detailed steps of NC-RIPM algorithm are given.

2.1 NC-RIPM algorithm for DOA estimation for Subarray 1

The array output of Subarray 1 for circular signals is

$$\boldsymbol{y}_1^{\mathrm{cir}}(t)=\boldsymbol{x}_1(t)=\boldsymbol{A}_1\boldsymbol{s}(t)+\bar{\boldsymbol{n}}_1^{\mathrm{cir}}(t) \tag{9}$$

where $\boldsymbol{A}_1\in\mathbf{R}^{M\times K}$

Similar to Eq.(3), we construct the extended array output of Subarray 1 as[18]

$$\boldsymbol{y}_1(t)=\begin{bmatrix}\boldsymbol{x}_1(t)\\ \boldsymbol{J}_{M1}\boldsymbol{x}_1^*(t)\end{bmatrix}=\boldsymbol{B}_1\boldsymbol{s}(t)+\bar{\boldsymbol{n}}_1(t) \tag{10}$$

where $\boldsymbol{B}_1\in\mathbf{R}^{2M\times K}$, $\bar{\boldsymbol{n}}_1(t)=\begin{bmatrix}\boldsymbol{n}_1(t)\\ \boldsymbol{J}_{M1}\boldsymbol{n}_1^*(t)\end{bmatrix}$. Compared with the circular signals, $\boldsymbol{B}_1$ has higher dimensions than $\boldsymbol{A}_1$, so the conjugate transpose information $\boldsymbol{x}_1^*(t)$ of the noncircular signals can be used.

The aperture of CSA for circular signals is

$$\gamma^{\mathrm{cir}}=1/2(\max(N(M-1)N,M(N-1))) \tag{11}$$

The aperture of CSA for noncircular signals is

$$\gamma^{\mathrm{noncir}}=(\max(N(M-1)N,M(N-1))) \tag{12}$$

The noncircular property doubles the aperture of the array, so it has better DOA estimation performance. $\boldsymbol{J}_{M1}$ is the permutation matrix and can be given as follows

$$\boldsymbol{J}_{M1}=\begin{bmatrix}0 & & 1\\ & \iddots & \\ 1 & & 0\end{bmatrix} \tag{13}$$

$$\boldsymbol{B}_1=\begin{bmatrix}\boldsymbol{A}_1\\ \boldsymbol{A}_1\boldsymbol{\Phi}_1\boldsymbol{\Psi}_1^{-2}\end{bmatrix} \tag{14}$$

where $\boldsymbol{\Phi}_1=\boldsymbol{\Gamma}_1^{-(M-1)}$ is a diagonal matrix, and

$$\boldsymbol{\Gamma}_1=\begin{bmatrix}\mathrm{e}^{\mathrm{j}\mu_{1,1}} & & \\ & \ddots & \\ & & \mathrm{e}^{\mathrm{j}\mu_{k,1}}\end{bmatrix} \tag{15}$$

Partition $\boldsymbol{B}_1$ can be given as follows

$$\boldsymbol{B}_1=\begin{bmatrix}\boldsymbol{B}_{x1}\\ \boldsymbol{B}_{y1}\end{bmatrix} \tag{16}$$

where $\boldsymbol{B}_{x1}\in\mathbf{C}^{K\times K}$ is a nonsingular matrix and $\boldsymbol{B}_{y1}\in\mathbf{C}^{(2M-K)\times K}$. From Ref.[19], $\boldsymbol{B}_{y1}$ is a linear transformation of $\boldsymbol{B}_{x1}$

$$\boldsymbol{P}_{c1}^{\mathrm{H}}\boldsymbol{B}_{x1}=\boldsymbol{B}_{y1} \tag{17}$$

where $\boldsymbol{P}_{c1}\in\mathbf{C}^{K\times(2M-K)}$ is the propagator matrix.

The covariance matrix of the extended array output can be expressed as follows

$$\boldsymbol{R}_1=E[\boldsymbol{y}_1(t)\boldsymbol{y}_1^{\mathrm{H}}(t)] \tag{18}$$

Partition $\boldsymbol{R}_1$ can be defined as follows[19]

$$\boldsymbol{R}_1=[\boldsymbol{G}_1,\boldsymbol{H}_1] \tag{19}$$

where $\boldsymbol{G}_1\in\mathbf{C}^{2M\times K}$ and $\boldsymbol{H}_1\in\mathbf{C}^{2M\times(2M-K)}$.

In the absence of noise, we can obtain

$$\boldsymbol{G}_1\boldsymbol{P}_{c1}=\boldsymbol{H}_1 \tag{20}$$

Define

$$\boldsymbol{P}_1=\begin{bmatrix}\boldsymbol{I}_{K1}\\ \boldsymbol{P}_{c1}^{\mathrm{H}}\end{bmatrix} \tag{21}$$

where $\boldsymbol{P}_1 \in \mathbf{C}^{2M \times K}$. According to Eqs. (16) and (17), we have

$$\boldsymbol{P}_1 \boldsymbol{B}_{x1} = \boldsymbol{B}_1 \tag{22}$$

In the case of noise, the propagator matrix can be estimated as follows

$$\hat{\boldsymbol{P}}_{c1} = \boldsymbol{G}_1^{+} \boldsymbol{H}_1 \tag{23}$$

Partition $\boldsymbol{P}_1$ can be split into two parts as follows

$$\boldsymbol{P}_1 = \begin{bmatrix} \boldsymbol{P}_{x1} \\ \boldsymbol{P}_{y1} \end{bmatrix} \tag{24}$$

where $\boldsymbol{P}_{x1} \in \mathbf{C}^{M \times K}$ and $\boldsymbol{P}_{y1} \in \mathbf{C}^{M \times K}$.

Define the selective matrices as follows

$$\boldsymbol{J}_{x1} = \begin{bmatrix} 1 & & 0 & 0 \\ & \ddots & & \vdots \\ 0 & & 1 & 0 \end{bmatrix}_{(M-1) \times M} \tag{25}$$

$$\boldsymbol{J}_{y1} = \begin{bmatrix} 0 & 1 & & 0 \\ \vdots & & \ddots & \\ 0 & 0 & & 1 \end{bmatrix}_{(M-1) \times M} \tag{26}$$

Let

$$\boldsymbol{P}_{a1} = \begin{bmatrix} \boldsymbol{J}_{x1} \boldsymbol{P}_{x1} \\ \boldsymbol{J}_{x1} \boldsymbol{P}_{y1} \end{bmatrix}, \quad \boldsymbol{P}_{b1} = \begin{bmatrix} \boldsymbol{J}_{y1} \boldsymbol{P}_{x1} \\ \boldsymbol{J}_{y1} \boldsymbol{P}_{y1} \end{bmatrix} \tag{27}$$

According to Eqs. (22), (24) and (27), we have

$$\boldsymbol{P}_{a1} \boldsymbol{B}_1 \boldsymbol{\Gamma}_1 = \boldsymbol{P}_{b1} \boldsymbol{B}_1 \tag{28}$$

Define

$$\boldsymbol{P}_{r1} = \boldsymbol{P}_{a1}^{+} \boldsymbol{P}_{b1} \tag{29}$$

According to Eqs. (28) and (29), we have

$$\boldsymbol{P}_{r1} = \boldsymbol{B}_1 \boldsymbol{\Gamma}_1 \boldsymbol{B}_1^{-1} \tag{30}$$

By performing the EVD of $\boldsymbol{P}_{r1}$, we can obtain

$$\boldsymbol{P}_{r1} = \boldsymbol{U}_1 \boldsymbol{\Lambda}_1 \boldsymbol{U}_1^{\mathrm{H}} \tag{31}$$

where $\boldsymbol{\Lambda}_1 = \mathrm{diag}\{[\eta_1, \cdots, \eta_K]\}$. Note that the eigenvalues of $\boldsymbol{P}_{r1}$ are corresponding to the diagonal elements of $\boldsymbol{\Gamma}_1$.

From Eqs. (1) and (2), the angle estimates of the k-th source can be obtained from Subarray 1 as follows

$$\sin\hat{\theta}_{k,1} = \frac{-\lambda \cdot \mathrm{angle}(\eta_k)}{\pi N} - \frac{2W_1}{N}$$
$$W_1 = 0, 1, \cdots, N-1 \tag{32}$$

The algorithm on Subarray 2 can be obtained in a similar way to that on Subarray 1. Note that the ambiguity problem arises because the inter-element spacing is larger than the half-wavelength, and ambiguity elimination is represented in the following sections.

2.2 DOA estimation and ambiguity elimination

Assume that there is $K = 1$ noncircular signal impinging on a CSA with the elevation angle $\theta = 20°$ and noncircular phase $\varphi = 10°$, where $M = 5$, $N = 3$ for the CSA, and SNR=20 dB. As shown in Fig.2, there are three estimated values for Subarray 1, and five estimated values for Subarray 2. In the set of estimated values of the two subarrays, the coincidence point is the real value.

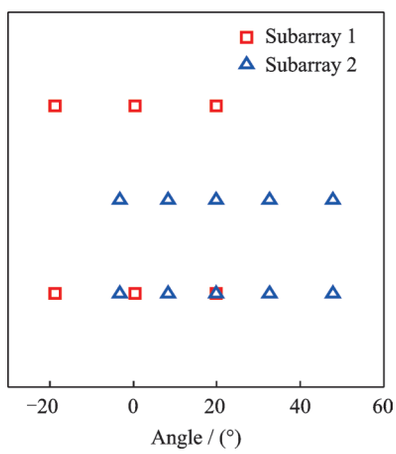

Fig.2 RIPM of the decomposed two subarrays

Assume there is only one far-field narrowband source impinging on the CSA from an elevation angle θ with NC phase φ. The phase difference between the received signals of two adjacent elements can be expressed as follows

$$\Delta = \mathrm{mod}\left(\frac{2\pi}{\lambda} d\sin\theta, 2\pi\right) \tag{33}$$

where the mod(·) operation returns the modulus after the division of parameter 1 by parameter 2. The mod operation is based on the principle that the phase of a signal rotates by 2π for every λ distance the signal travels. Therefore, the relationship between the phase difference and the element spacing is given as follows[13]

$$\Delta + 2k\pi = \frac{2\pi}{\lambda} d\sin\theta \tag{34}$$

where k is an integer. Since $\theta \in [-\pi/2, \pi/2]$, we have $-1 \leqslant \sin\theta \leqslant 1$. Therefor, k is in the range of $\left[-\frac{d}{\lambda} - \frac{\Delta}{2\pi}, \frac{d}{\lambda} - \frac{\Delta}{2\pi}\right]$. For particular phase differences Δ, there exists one or a set of DOAs that

satisfy Eq. (34). Specifically, in the case of $d \leqslant \lambda/2$, k can only be 0. As d increases, the number of possible k values increases.

In a CSA, the spacing between two adjacent sensors of each subarray is much larger than the half-wavelength. Therefore, there are multiple ambiguous DOAs in addition to the actual one[13].

Suppose θ_k is the actual DOA of the NC signal and θ_k^a is one of the ambiguous DOAs. The NC phase φ is negligible to the angle ambiguity. According to Eq.(34), the relationship between the actual DOA θ_k and its ambiguous DOA θ_k^a for Subarray 1 and Subarray 2 is given as follows

$$\sin\theta_{k,1} - \sin\theta_{k,1}^a = \frac{2P}{N} \tag{35}$$

$$\sin\theta_{k,2} - \sin\theta_{k,2}^a = \frac{2Q}{M} \tag{36}$$

where P is the difference between any elements of set k, which is an integer between $(-N+1)$ and $(N-1)$, and Q is an integer between $(-M+1)$ and $(M-1)$, respectively. Considering that θ_k and θ_k^a are interchangeable, there is a total of $(N-1)$ ambiguous angles for Subarray 1. Similarly, there are totally $(M-1)$ ambiguous angles for Subarray 2.

Although ambiguity arises with the enlarge of the inter-element spacing, the correct estimation can be achieved by finding the common results of the N and M estimations based on the coprimeness of N and M, and the proof process refers to Ref. [15]. In the noise case, the correct estimations will not be strictly overlapped, and the actual DOA is estimated by averaging two closest solutions as follows

$$\hat{\theta}_k = \frac{\hat{\theta}_{k,1} + \hat{\theta}_{k,2}}{2} \quad k = 1, \cdots, K \tag{37}$$

where $\hat{\theta}_{k,1}$ and $\hat{\theta}_{k,2}$ denote the corresponding angles of the two closest solutions of the two decomposed subarrays.

2.3 Detailed steps of NC-RIPM algorithm

According to Eq.(10), the covariance matrix of a sample extended with finite array output data can be expressed as follows

$$\hat{\boldsymbol{R}} = \frac{1}{L}\sum_{l=1}^{L} \boldsymbol{y}(t_l)\,\boldsymbol{y}^{\mathrm{H}}(t_l) \tag{38}$$

The main steps of the NC-RIPM algorithm are as follows:

(1) Construct the extended matrix $\boldsymbol{y}$ using Eq.(10), then calculate the covariance matrix $\hat{\boldsymbol{R}}$ of Subarray 1 and Subarray 2.

(2) Compute the propagator matrix $\boldsymbol{P}_c$, and obtain $\boldsymbol{P}_r$ using Eq.(30).

(3) Perform EVD of $\boldsymbol{P}_r$ using Eq.(31).

(4) Estimate the ambiguous angles using Eq.(32).

(5) Select the K nearest angles as the estimates based on Eq.(37).

3 Performance Analysis

In this section, we first discuss the extension of array DOF, we then analyze the computational complexity of the proposed method, and finally, we derive the CRB of DOA estimation for NC signals.

3.1 Degree of freedom

The DOF is the maximum number of signal sources the array can estimate[19]. For CSA, it is determined by the subarray with fewer elements. Therefor, the DOF of a CSA for circular signals is given as follows[16]

$$\mathrm{DOF}_{\mathrm{CSA}}^{\mathrm{cir}} = \min(M,N) - 1 \tag{39}$$

In this paper, the NC property of incident signals has been considered, which can double the number of sources that can be estimated. Therefore, we can increase the DOF of CSA to

$$\mathrm{DOF}_{\mathrm{CSA}}^{\mathrm{noncir}} = 2\min(M,N) - 1 \tag{40}$$

Figs.3, 4 depict the DOA estimation results of the RIPM for NC signals and circular signals, respectively, over 100 trials, where the actual DOAs are 10° and 24°, respectively, and SNR= 5 dB, $M = 2$, and $N = 3$. It is shown that the proposed algorithm can accurately estimate the two angles, while the RIPM algorithm fails to obtain the correct results when the signals are circular.

3.2 Complexity analysis

In this section, we consider only the complexity of the algorithms with Subarray 1. Table 1 shows the comparison of the computational complexity of

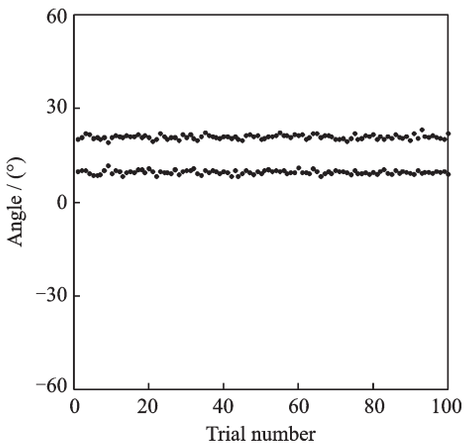

Fig.3 RIPM for noncircular signals

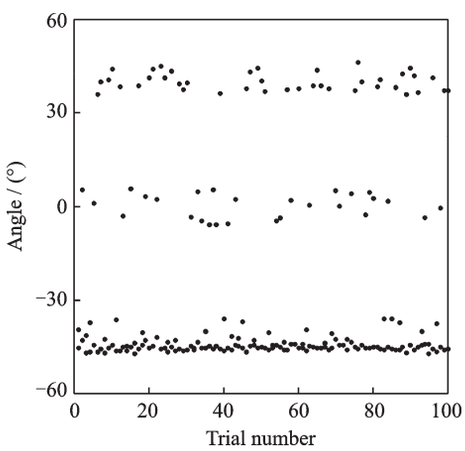

Fig.4 RIPM for circular signals

Table 1 Computational complexity of NC-RIPM, NC-Capon, and NC-ESPRIT algorithms for CSA

Algorithm	Computational complexity
NC-RIPM	$O\left(8MK^2+3K^3-6K^2+4M^2(L+K)\right)+\left(8NK^2+3K^3-6K^2+4N^2(L+K)\right)$
NC-Capon	$O\left(4M^2L+8M^3+\left(8M^2+8M\right)n_1\right)+\left(4N^2L+8N^3+\left(8N^2+8N\right)n_2\right)$
NC-ESPRIT	$O\left(8(M-1)K^2+13K^3+8M^3+4M^2L\right)+\left(8(N-1)K^2+13K^3+8N^3+4N^2L\right)$

the proposed algorithm with those of NC-ESPRIT[18] and NC-Capon[15] algorithms, where n_1 and n_2 denote the spectral searching times of Subarray 1 and Subarray 2. Table 2 shows the comparison of average running time versus M of NC-RIPM, NC-Capon, and NC-ESPRIT algorithms for CSA. The computational complexity comparisons versus L and M are shown in Figs. 5, 6, respectively. As shown in Fig. 6, the proposed algorithm has a lower computational complexity than the NC-Capon and NC-ESPRIT algorithms.

Table 2 Comparison of average running time versus M of NC-RIPM, NC-Capon, and NC-ESPRIT algorithms for CSA s

Algorithm	$M=4$ $N=3$	$M=5$ $N=4$	$M=6$ $N=5$	$M=7$ $N=6$
NC-RIPM	0.170	0.176	0.179	0.207
NC-Capon	9.770	10.842	11.741	13.869
NC-ESPRIT	0.175	0.188	0.187	0.216

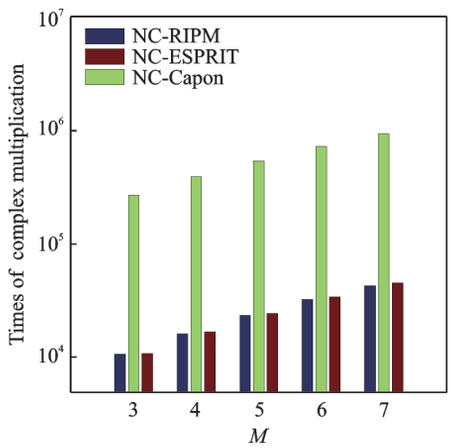

Fig.5 Comparison of computational complexities versus M

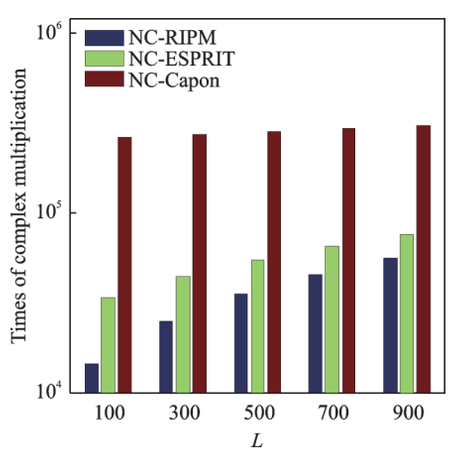

Fig.6 Comparison of computational complexities versus snapshots

3.3 Crámer-Rao bound

In the case of finite samples, the extended data model of NC signals for both subarrays can be presented as follows[10]

$$\boldsymbol{y}(t)=\begin{bmatrix}\boldsymbol{x}(t)\\ \boldsymbol{x}^*(t)\end{bmatrix} \tag{41}$$

where $\boldsymbol{x}(t)=[\,\boldsymbol{x}_1^{\mathrm{T}}(t),\boldsymbol{x}_1^{\mathrm{T}}(t)\,]^{\mathrm{T}}$.

According to the probability density function of $\boldsymbol{y}(t)$[20]

$$p(u,v)=p'(\boldsymbol{y})=$$
$$\pi^{-G}[\det(\boldsymbol{R}_y)]^{-1/2}\exp\left[-\frac{1}{2}\boldsymbol{y}^{\mathrm{H}}\boldsymbol{R}_y^{-1}\boldsymbol{y}\right] \quad (42)$$

where $G=M+N-1$ is the total number of sensors in an array, and

$$\boldsymbol{R}_y=E\{\boldsymbol{y}(t)\boldsymbol{y}^{\mathrm{H}}(t)\}=\boldsymbol{B}\boldsymbol{R}_s\boldsymbol{B}^{\mathrm{H}}+\sigma_n^2\boldsymbol{I}_{2M} \quad (43)$$

with $\boldsymbol{R}_s=\begin{bmatrix}\boldsymbol{R}_s & \boldsymbol{R}'_s\\ \boldsymbol{R}'^{*}_s & \boldsymbol{R}^{*}_s\end{bmatrix}$, $\boldsymbol{R}_s=E\{\boldsymbol{s}(t)\boldsymbol{s}^{\mathrm{H}}(t)\}$, $\boldsymbol{R}'_s=E\{\boldsymbol{s}(t)\boldsymbol{s}^{\mathrm{T}}(t)\}$, and $\boldsymbol{B}=\begin{bmatrix}\boldsymbol{A} & \boldsymbol{0}\\ \boldsymbol{0} & \boldsymbol{A}^{*}\end{bmatrix}$.

Consequently, the CRB of NC sources for a CSA can be expressed as follows[20-22]

$$\mathrm{CRB}^{\mathrm{noncir}}=\frac{\sigma_n^2}{2}\cdot$$
$$\left\{\mathrm{Re}\left[\boldsymbol{D}^{\mathrm{H}}\boldsymbol{\Pi}_{\boldsymbol{A}}^{\perp}\boldsymbol{D}\odot\left([\boldsymbol{R}_s\boldsymbol{A}^{\mathrm{H}},\boldsymbol{R}'_s\boldsymbol{A}^{\mathrm{T}}]\mathrm{R}_{\bar{y}}^{-1}\begin{bmatrix}\boldsymbol{A}\boldsymbol{R}_s\\ \boldsymbol{A}^{*}\boldsymbol{R}'^{*}_s\end{bmatrix}\right)^{\mathrm{T}}\right]\right\}^{-1} \quad (44)$$

where $\boldsymbol{D}=\mathrm{d}\boldsymbol{A}(\Theta_1)/\mathrm{d}\Theta_1$, $\boldsymbol{\Pi}^{\perp}_{\boldsymbol{A}(\Theta_1)}$ is the projection matrix $\boldsymbol{A}[\boldsymbol{A}^{\mathrm{H}}\boldsymbol{A}]^{-1}\boldsymbol{A}^{\mathrm{H}}$, $\boldsymbol{R}_{\bar{y}}=\begin{bmatrix}\boldsymbol{R}_y & \boldsymbol{R}'_y\\ \boldsymbol{R}'^{*}_y & \boldsymbol{R}^{*}_y\end{bmatrix}$, and $\odot$ is the Hadamard product (i.e., $(\boldsymbol{A}\odot\boldsymbol{B})_{i,j}=(\boldsymbol{A})_{i,j}(\boldsymbol{B})_{i,j}$).

3.4 Advantages of the proposed algorithm

Compared with conventional RIPM algorithm, the proposed algorithm has the following advantages:

(1) The proposed algorithm has a much lower computational complexity as no spectral peak search is involved.

(2) The proposed algorithm can obtain a larger array aperture and more DOFs. Specifically, the maximum number of detected sources is increased to $\min(2M-1,2N-1)$.

(3) It can achieve a better DOA estimation performance than Capon method and ESPRIT-based method.

(4) The proposed algorithm can work well without estimating the NC phase.

These advantages are verified in the simulation section below.

4 Simulation Results

Independent Monte Carlo simulations are used to evaluate the DOA estimation performance. The root mean square error (RMSE) is defined as follows

$$\mathrm{RMSE}=\frac{1}{K}\sum_{k=1}^{K}\sqrt{\frac{1}{L}\sum_{l=1}^{L}[\hat{\theta}_{k,l}-\theta_k]^2} \quad (45)$$

where θ_k is the real angle of the k-th signal and $\hat{\theta}_{k,n}$ is the estimate of θ_k in the l-th Monte Carlo trial, where $l=1,2,\cdots,L$. All the numerical results were obtained from $L=1\,000$ independent trials.

4.1 DOA estimation performance improvement by using NC features

In Fig.7, we show the DOA estimation performance of circular and NC sources versus SNR for CSA. Assume that there are $K=2$ NC signals impinging on the CSA with elevation angles being $\theta=(10°,30°)$ and the NC phases being $\varphi=(5°,15°)$, and the number of sensors for Subarray 1 and Subarray 2 is set as $M=5$ and $N=7$, respectively. Fig.7 shows that the proposed algorithm NC-RIPM achieves a much better performance than conventional RIPM for circular signals.

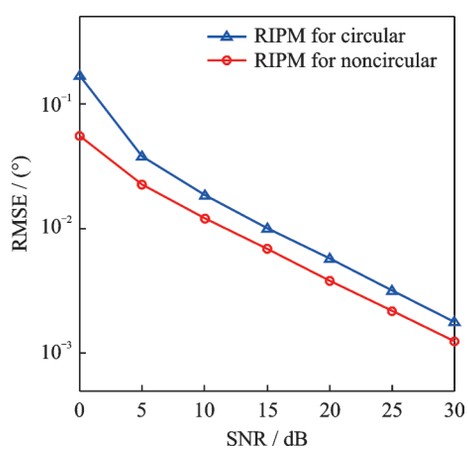

Fig.7 RMSE performance comparison with circular and noncircular signals versus SNR

4.2 DOA estimation performance improvement by using coprimeness

Consider that $K=2$ uncorrelated NC signals impinge on a ULA and a CSA. For fair comparison, the ULA has $M+N-1$ sensors. Fig.8 indicates the RMSE performance of the NC-RIPM for ULA and NC-RIPM for CSA. The CRB[22] is plot-

ted as a benchmark. It is illustrated in Fig.8 that the proposed algorithm has a better DOA estimation performance for CSA than for ULA.

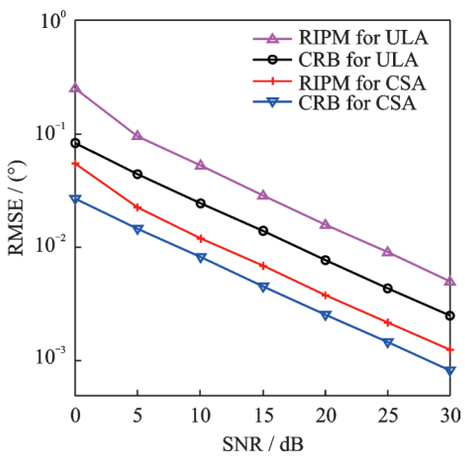

Fig. 8 RMSE performance comparison versus different array geometries

4.3 Comparison of DOA estimation RMSE versus Different algorithms

Fig.9 indicates the DOA estimation performance comparison among the RIPM, RD-Capon, and ESPRIT for CSA. It can be seen that the proposed algorithm has approximate DOA estimation performance.

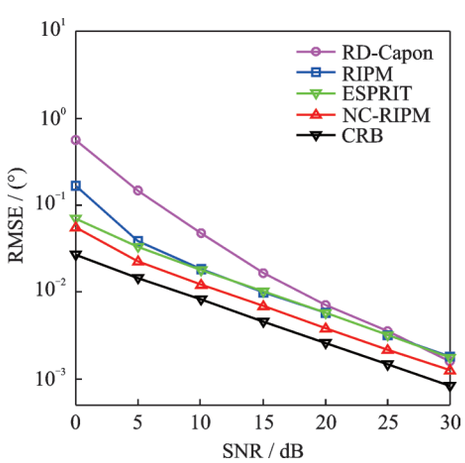

Fig.9 DOA estimation performance comparison versus SNR

Fig.10 presents the DOA estimation performance of different methods versus different snapshots. In this simulation, we fix $M=7$, $N=5$. Fig.10 shows that the DOA estimation performance becomes better with the increase in snapshot. The reason is that increasing the amount of sampled data makes the covariance matrix more accurate.

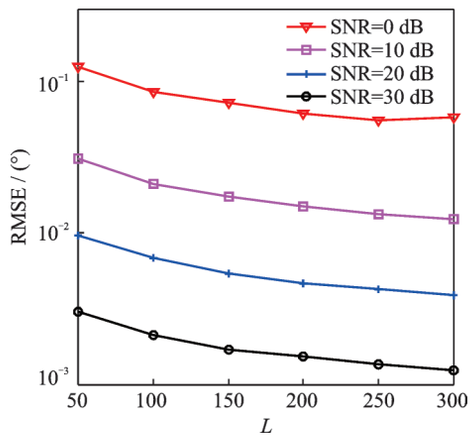

Fig.10 DOA estimation performance comparison versus snapshot number

4.4 Comparison of DOA estimation RMSE versus different Parameters

Fig.11 plots the variation tendency of DOA estimation performance with a changing sensor number of Subarray 1, while the sensor number of Subarray 2 is fixed.

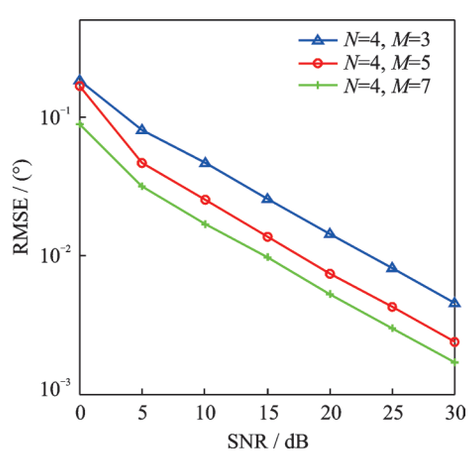

Fig.11 DOA estimation performance comparison versus M

5 Conclusions

In this paper, we proposed the NC-RIPM algorithm for the DOA estimation of NC signals for CSA. Compared with the conventional RIPM for circular signals and NC-RIPM for ULA, the proposed algorithm has a better estimation performance by exploiting the NC property and the coprimeness of the subarrays. Different from the conventional PM method, the proposed algorithm achieves DOA

estimations without performing the spectral peak search. It has a much lower computational complexity. Moreover, the proposed algorithm requires no EVD of the covariance matrix, and it works well without estimating the NC phases. Numerical simulation results verify the effectiveness and improvement of the proposed algorithm.

References

[1] GARDNER W A. Simplication of MUSIC and ESPRIT by exploitation of cyclostationarity[J]. Proceedings of the IEEE, 1988, 76(7): 845-847.

[2] SCHMIDT R O. Multiple emitter location and signal parameter estimation[J]. IEEE Trans Antennas and Propagation, 1986, 34(3): 276-280.

[3] ZOLTOWSKI M D, HAARDT M, MATHEWS C P. Closed-form 2D angle estimation with rectangular arrays in element space or beamspace via unitary ESPRIT[J]. IEEE Trans Signal Process, 1996, 44(1): 326-328.

[4] MARCOS S, MARSAL A, BENIDIR M. The propagator method for source bearing estimation[J]. Signal Processing, 1995, 42(2): 121-138.

[5] STOICA P, HÄNDEL P, SÖDERSTRÖM T. Study of Capon method for array signal processing[J]. Circuits, Systems and Signal Processing, 1995, 14(6): 749-770.

[6] ZHANG X F, WU H L, LI J F, et al. Computationally efficient DOD and DOA estimation for bistatic MIMO radar with propagator method[J]. International Journal of Electronics, 2012, 99(9): 1207-1221.

[7] TAYEM N, KWON H M. L-shape 2-dimensional arrival angle estimation with propagator method[J]. IEEE Trans Antennas and Propagation, 2005, 53(5): 1622-1630.

[8] ABEIDA H, DELMAS J P. MUSIC-like estimation of direction of arrival for noncircular sources[J]. IEEE Trans Signal Processing, 2006, 54(7): 2678-2690.

[9] GAO F, NALLANATHAN A, WANG Y. Improved MUSIC under the coexistence of both circular and noncircular sources[J]. IEEE Trans Signal Processing, 2008, 56(7): 3033-3038.

[10] ZOUBIR A, CHARGE P, WANG Y. Non circular sources localization with ESPRIT[C]//The 6th European Conference on Wireless Technology. Munich, Germany: IEEE, 2003.

[11] ZHANG X F, CAO, R Z, ZHOU M. Noncircular PARAFAC for 2D-DOA estimation of noncircular signals in arbitrarily spaced acoustic vector-sensor array subjected to unknown locations[J]. Eurasip Journal on Advances in Signal Processing, 2013(1): 107.

[12] PAL P , VAIDYANATHAN P P. Nested arrays: A novel approach to array processing with enhanced degrees of freedom[J]. IEEE Trans Signal Processing, 2010, 58(8): 4167-4181.

[13] WU Q, SUN F, DING G, et al. Two-dimensional direction-of-arrival estimation for co-prime planar arrays: A partial spectral search approach[J]. IEEE Sensors Journal, 2016, 16(14): 5660-5670.

[14] LI J, WANG F, JIANG D. DOA estimation based on real-valued cross correlation matrix of coprime arrays[J]. Sensors, 2017, 17(3): 638.

[15] ZHAI Hui, ZHANG Xiaofei, ZHENG W. DOA estimation for noncircular signals with coprime linear array via locally reduced dimensional capon[J]. International Journal of Electronics, 2017: 10.12783/dtcse/cece2017/14593.

[16] ZHOU C W, SHI Z G, GU Y J, et al. DECOM: DOA estimation with combined Capon for coprime array[C]//2013 International Conference on Wireless Communications and Signal Processing. Hangzhou, China: IEEE, 2013.

[17] FU X W, CAO R Z, WEN F Q. A de-noising 2D-DOA estimation method for uniform rectangle array[J]. IEEE Communications Letters, 2018, 22(9): 1854-1857.

[18] ZHAI Hui, ZHANG Xiaofei, ZHENG Wang. DOA estimation of noncircular signals with combined ESPRIT for coprime linear array[C]//CECE 2017. Sanya, China:[s.n.], 2017.

[19] CHEN X Q, WANG C H, ZHANG X F. DOA and noncircular phase estimation of noncircular signal via an improved noncircular rotational invariance propagator method[J]. Mathematical Problems in Engineering, 2015, 2015: 235173.

[20] STOICA P, NEHORAI A. Performance study of conditional and unconditional direction of arrival estimation[J]. IEEE Trans Acoust, Speech, Signal Processing, 1990, 38(10): 1783-1795.

[21] PICINBONO B. Second-order complex random vectors and normal distributions[J]. IEEE Trans Signal Processing, 1996, 44(10): 2637-2640.

[22] DELMAS J-P , ABEIDA H. Stochastic Cramér-Rao bound for noncircular signals with application to DOA estimation[J]. IEEE Trans Signal Processing, 2004, 52(11): 3192-3198.

Acknowledgements This work was supported by the National Natural Science Foundations of China (Nos.61371169,

61601167, 61601504), the Natural Science Foundation of Jiangsu Province (No.BK20161489), the Open Research Fund of State Key Laboratory of Millimeter Waves, Southeast University (No. K201826), and the Fundamental Research Funds for the Central Universities (No. NE2017103).

Authors Mr. **ZHAI Hui** is currently pursuing the Ph.D. degree in communication and information systems of College of Electronic and Information Engineering, Nanjing University of Aeronautics and Astronautics. His current research interests include array signal processing and detection.

Ms. **CHEN Weiyang** is currently a Ph.D. of College of Electronic and Information Engineering in Nanjing University of Aeronautics and Astronautics. His research is focused on array signal processing and acoustic vector sensor array.

Prof. **ZHANG Xiaofei** is currently a professor of College of Electronic and Information Engineering in Nanjing University of Aeronautics and Astronautics. His research is focused on array signal processing and communication signal processing.

Mr. **ZHENG Wang** is currently pursuing the Ph.D. degree in communication and information systems of College of Electronic and Information Engineering, Nanjing University of Aeronautics and Astronautics. His current research interests include array signal processing and detection.

Author contributions Mr. **ZHAI Hui** contributed to the background of the study, designed the study. Ms. **CHEN Weiyang** wrote the manuscript. Prof. **ZHANG Xiaofei** contributed to the discussion and analysis. Mr. **ZHENG Wang** contributed to the simulation and prepared all drafts.

Competing interests The authors declare no competing interests.

(Production Editor: Zhang Huangqun)